ATLAS NOTE

ATLAS-CONF-2014-049

July 21, 2014

Search for neutral Higgs bosons of the Minimal Supersymmetric Standard Model in pp collisions at $\sqrt{s} = 8$ TeV with the ATLAS detector

The ATLAS Collaboration

Abstract

A search for the neutral Higgs bosons predicted by the Minimal Supersymmetric Standard Model (MSSM) is reported. The analysis is performed on data from proton-proton collisions at a centre-of-mass energy of 8 TeV collected with the ATLAS detector at the Large Hadron Collider (LHC). The sample was collected in 2012 and corresponds to an integrated luminosity of 19.5–20.3 fb^{-1}. The MSSM Higgs bosons are searched for in the $\tau^+\tau^-$ final state. No significant excess over the expected background is observed, and exclusion limits are derived for the production cross section times branching fraction of a scalar particle as a function of its mass. The results are also interpreted in the MSSM parameter space by quoting exclusion limits on $\tan\beta$ as a function of m_A.

ATLAS-CONF-2014-049
21 July 2014

1 Introduction

The discovery of a scalar particle with a mass of about 125 GeV at the Large Hadron Collider (LHC) [1,2] has provided important insight into the mechanism of electroweak symmetry breaking. Experimental studies of the new particle [3–7] demonstrate consistency with the Standard Model (SM) Higgs boson [8–13]. However, it remains possible that the discovered particle is part of an extended scalar sector, a scenario that is favoured by a number of theoretical arguments [14, 15].

The Minimal Supersymmetric Standard Model (MSSM) [16–20] is an extension of the SM which provides a framework addressing naturalness, gauge coupling unification and the existence of dark matter. The MSSM is compatible with the recently discovered Higgs boson at the LHC (see, e.g. Ref. [21–23]). The Higgs sector of the MSSM contains two Higgs doublets, which results in five physical Higgs bosons after electroweak symmetry breaking. Of these bosons, two are neutral and CP-even (h, H),[1] one is neutral and CP-odd (A), and the remaining two are charged ($H^{\pm}$). Only two additional parameters are needed with respect to the SM at tree level to describe the MSSM Higgs sector and can be chosen to be the mass of the CP-odd Higgs boson, m_{A}, and the ratio of the vacuum expectation values of the two Higgs doublets, $\tan\beta$. The couplings of the MSSM Higgs bosons to down-type fermions are enhanced with respect to the SM, especially for large $\tan\beta$ values, resulting in increased branching fractions to τ leptons and b-quarks, as well as a higher cross section for Higgs boson production in association with b-quarks. Previous searches for a neutral MSSM Higgs boson have been performed at LEP [24], the Tevatron [25–27] and the LHC [28–30].

This note presents the results of a search for a neutral MSSM Higgs boson in the $\tau\tau$ decay mode using 19.5–20.3 fb^{-1} of proton–proton collision data collected with the ATLAS detector [31] in 2012 at a centre-of-mass energy of 8 TeV. Higgs boson production through gluon fusion or in association with b-quarks is considered (see Fig. 1), with the latter mode dominating for high $\tan\beta$ values. The results of the search are interpreted in the m_h^{max} scenario [32, 33] of the MSSM.

The search for the SM Higgs boson in the $\tau\tau$ channel at the LHC [34, 35] is similar to that described here. The important difference between the two searches is that they are optimised for different production mechanisms and different Higgs boson mass ranges. As a consequence, this search has little sensitivity to the production of a SM Higgs boson with mass around 125 GeV. For consistency the SM Higgs signal is not considered part of the SM background, as the MSSM contains a SM-like Higgs boson for large parts of the parameter space.

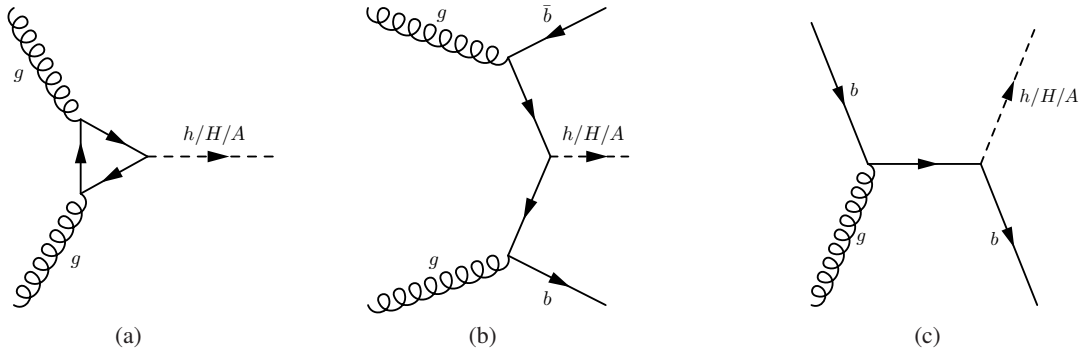

Figure 1: Example Feynman diagrams for gluon-fusion (a) and b-associated production in the four-flavour scheme (b) and five-flavour scheme (c) of a neutral MSSM Higgs boson.

[1] By convention the lighter CP-even Higgs boson is denoted h, the heavier CP-even Higgs boson is denoted H. The masses of the three bosons are denoted in the following as m_h, m_H and m_A for h, H and A respectively.

2 The ATLAS detector

The ATLAS experiment [31] at the LHC is a multi-purpose particle detector with a forward-backward symmetric cylindrical geometry and a near 4π coverage in solid angle. It consists of an inner tracking detector surrounded by a thin superconducting solenoid providing a 2 T axial magnetic field, electromagnetic and hadronic calorimeters, and a muon spectrometer. The inner tracking detector covers the pseudorapidity range[2] $|\eta| < 2.5$. It consists of silicon pixel, silicon micro-strip, and transition radiation tracking detectors. Lead/liquid-argon (LAr) sampling calorimeters provide electromagnetic (EM) energy measurements with high granularity. A hadronic (iron/scintillator-tile) calorimeter covers the central pseudorapidity range ($|\eta| < 1.7$). The end-cap and forward regions are instrumented with LAr calorimeters for both EM and hadronic energy measurements up to $|\eta| = 4.9$. The muon spectrometer surrounds the calorimeters and is based on three large air-core toroid superconducting magnets with eight coils each. Its bending power is in the range from 2.0 to 7.5 Tm. It includes a system of precision tracking chambers and fast detectors for triggering. A three-level trigger system is used to select events. The first-level trigger is implemented in hardware and uses a subset of the detector information to reduce the accepted rate to at most 75 kHz. This is followed by two software-based trigger levels that together reduce the accepted event rate to 400 Hz on average depending on the data-taking conditions during 2012.

3 Data and Monte Carlo simulation samples

The data used in this search were recorded by the ATLAS experiment during the 2012 LHC run with proton–proton collisions at a centre-of-mass energy of 8 TeV. They correspond to an integrated luminosity of 19.5–20.3 fb^{-1}, depending on the event topology.

Simulated samples of signal and background events were produced using various event generators. The presence of multiple interactions occurring in the same or neighbouring bunch crossings (pileup) was accounted for, and the ATLAS detector was modelled using GEANT4 [36, 37].

The Higgs boson production mechanisms considered in this analysis are gluon-fusion and b-associated production. The cross sections for these processes have been calculated using HIGLU [38], ggh@nnlo [39] and SusHi [40]. For b-associated production, four-flavour [41, 42] and five-flavour [43] cross section calculations are combined [44]. The masses, couplings and branching ratios of the Higgs bosons are computed with FeynHiggs [45]. Gluon-fusion production is simulated with POWHEG [46], while b-associated production is simulated with SHERPA [47]. Both samples use the CT10 [48] parton distribution function set. The signal samples are generated at discrete values of m_{A}, with the mass step chosen by taking the $\tau\tau$ mass resolution into account. The signal model is constructed by combining three mass samples, one for each of the h, H and A bosons, with appropriately scaled cross sections and branching ratios. The cross sections, branching ratios, as well as the masses of h and H bosons depend on m_{A}, $\tan\beta$ and the MSSM scenario under study.

Background samples of W and Z bosons produced in association with jets are produced using ALPGEN [49], while the high mass Z/γ^* tail is modelled separately using PYTHIA8 [50, 51] since a higher statistics sample was available and in the high mass range the current analysis is rather insensitive to the modelling of b-jet production. WW production is modelled with ALPGEN and WZ and ZZ production is modeled with HERWIG [52]. Top pair production uses POWHEG and MC@NLO [53], and single-top

[2] ATLAS uses a right-handed coordinate system with its origin at the nominal interaction point (IP) in the centre of the detector and the z-axis along the beam pipe. The x-axis points from the IP to the centre of the LHC ring, and the y-axis points upwards. Cylindrical coordinates (r, ϕ) are used in the transverse plane, ϕ being the azimuthal angle around the beam pipe. The pseudorapidity is defined in terms of the polar angle θ as $\eta = -\ln\tan(\theta/2)$. Angular distance is measured in units of $\Delta R \equiv \sqrt{\Delta\eta^2 + \Delta\phi^2}$.

processes are generated with AcerMC [54]. All simulated background samples use the CTEQ6L1 [55] parton distribution function set apart from MC@NLO that uses CT10.

For all the simulated event samples, the parton shower and hadronisation are simulated with HERWIG, PYTHIA8 or SHERPA. PYTHIA8 is used for POWHEG generated samples, SHERPA for the b-associated signal production and HERWIG for the remaining samples. Decays of τ leptons are generated with TAUOLA [56], SHERPA or PYTHIA8. PHOTOS [57] or SHERPA provides additional radiation from charged leptons.

$Z/\gamma^* \to \tau\tau$ events form an irreducible background that is particularly important when considering low mass Higgs bosons ($m_A \lesssim 200$ GeV). It is modelled with $Z/\gamma^* \to \mu^+\mu^-$ events from data, where the muon tracks and the associated calorimeter cells are replaced by the corresponding simulated signature of a τ lepton decay. The two τ leptons are simulated by TAUOLA. The procedure takes into account the effect of τ polarisation and spin correlations. In the resulting sample, the τ lepton decays and their detector response are modelled by the simulation, while the underlying event kinematics and all other properties are obtained from data. Although the $\mu\mu$ event selection in data results in a pure $Z/\gamma^* \to \mu^+\mu^-$ sample, there is still some contributions from $t\bar{t}$ and diboson production, which is taken into account using simulation. This τ-embedded $Z/\gamma^* \to \mu^+\mu^-$ sample has been validated as described in Refs. [28, 58].

4 Object reconstruction

Electron candidates are formed from energy deposits in the electromagnetic calorimeter associated with a charged particle track measured in the inner detector. Electrons are selected if they have a transverse energy $E_{\mathrm{T}} > 15$ GeV, lie within $|\eta| < 2.47$, but outside the transition region between the barrel and end-cap calorimeters ($1.37 < |\eta| < 1.52$), and meet the "medium" identification requirements defined in Ref. [59]. Additional isolation criteria, based on tracking and calorimeter information, are used to suppress backgrounds from misidentified jets or semi-leptonic decays of heavy quarks. In particular, the sum of the calorimeter deposits in cones of sizes $\Delta R = 0.2 - 0.3$ with respect to the electron direction is required to be less than 6–14% of the electron E_{T} depending on the channel. Similarly, the scalar sum of the transverse momentum of tracks with $p_{\mathrm{T}} > 1$ GeV in cones of sizes $\Delta R = 0.3 - 0.4$ with respect to the electron direction is required to be less than 6–13% of the electron track p_{T} depending on the channel.

Muon candidates are reconstructed by associating an inner detector track with a muon spectrometer track [60]. For this analysis, the reconstructed muons are required to have a transverse momentum $p_{\mathrm{T}} > 10$ GeV and to lie within $|\eta| < 2.5$. Additional track quality and isolation criteria are required to further suppress backgrounds from cosmic rays, hadrons punching through the calorimeter, or muons from semi-leptonic decays of heavy quarks. The muon calorimetric and track isolation criteria use the same cone sizes and the same threshold values with respect to the muon p_{T} as in the case of electrons.

Jets are reconstructed using the anti-k_t algorithm [61] with a radius parameter $R = 0.4$, taking topological clusters [62] in the calorimeter as input. The jet energy is calibrated using a combination of test-beam results, simulation and *in situ* measurements [63]. Jets must satisfy $E_T > 20$ GeV and $|\eta| < 4.5$. To reduce the effect of pile-up, it is required that, for jets within $|\eta| < 2.4$ and $E_{\mathrm{T}} < 50$ GeV, at least half of the transverse momentum, as measured by the associated charged particles, be from particles matched to the primary vertex[3].

A multivariate discriminant is used to tag jets, reconstructed within $|\eta| < 2.5$, originating from a b-quark [64]. The b jet identification has an average efficiency of 70% in simulated $t\bar{t}$ events whereas the corresponding light-quark jet misidentification probability is approximately 0.7%, but varies as a function of the jet p_{T} and η [65].

[3]Proton-proton collision vertices are reconstructed in ATLAS by requiring that at least five tracks with $p_{\mathrm{T}} > 0.4$ GeV are associated to a given vertex. The primary vertex is taken to be the reconstructed vertex with the highest summed track p_{T}^2.

Hadronic decays of τ leptons (τ_{had}) [66] are reconstructed starting from topological clusters in the calorimeter. A τ_{had} candidate must lie within $|\eta| < 2.5$, have a transverse momentum greater than 20 GeV, one or three associated tracks and a charge of ± 1. Information on the collimation, isolation, and shower profile is combined into a multivariate discriminant against backgrounds from jets. Dedicated algorithms that reduce the number of electrons and muons misreconstructed as hadronic tau decays are applied. In this analysis, two τ_{had} identification selections are used —"loose" and "medium"— with efficiencies of about 65% and 55%, respectively. The rejection against jets misreconstructed as τ_{had} of these criteria depends on τ_{had} p_{T}, η, the number of associated tracks and whether the jet is quark or gluon initiated. For "loose" identification, it is about 10 and 20 for τ_{had} with one and three associated tracks, respectively, as measured in a sample of multi-jet events in data [66]. The rejection factors become, respectively, 50 and 100 for "medium" identification criterion.

When different objects selected according to the criteria mentioned above overlap with each other geometrically (within $\Delta R = 0.2$) only one of them is considered. The overlap is resolved by selecting muon, electron, τ_{had} and jet candidates in this order of priority.

The missing transverse momentum, $E_{\text{T}}^{\text{miss}}$, is defined as the magnitude of the negative vectorial sum of muons and energy deposits in the calorimeters [67]. The direction of this vectorial sum defines the $E_{\text{T}}^{\text{miss}}$ direction. Clusters of calorimeter-cell energy deposits belonging to jets, τ_{had} candidates, electrons, and photons, as well as cells that are not associated to any object, are treated separately in the $E_{\text{T}}^{\text{miss}}$ calculation. Calorimenter cells, which are not matched to any object, are weighted by the fraction of unmatched tracks that are associated to the primary vertex, in order to reduce the effect of pile-up on the $E_{\text{T}}^{\text{miss}}$ resolution. The contributions of muons to $E_{\text{T}}^{\text{miss}}$ are calculated differently for isolated and non-isolated muons, to account for the energy deposited by muons in the calorimeters.

5 Search Channels

The following $\tau\tau$ decay modes are considered in this search: $\tau_{\text{e}}\tau_{\mu}$ (6%), $\tau_{\text{e}}\tau_{\text{had}}$ (23%), $\tau_{\mu}\tau_{\text{had}}$ (23%) and $\tau_{\text{had}}\tau_{\text{had}}$ (42%), where τ_{e} and τ_{μ} represent the two leptonic tau decay modes and the percentages in the parentheses denote the corresponding $\tau\tau$ branching ratios. The selections defined for each of the channels and described in Sections 5.1–5.3 are such that there are no common events in any two of these channels.

Events are collected using a number of single and combined object triggers. The single electron and muon triggers require an isolated lepton with a p_{T} threshold of 24 GeV. The single τ_{had} trigger implements a τ_{had} with a p_{T} threshold of 125 GeV. The following combined object triggers are used: an electron-muon trigger with lepton p_{T} thresholds of 12 and 8 GeV for electrons and muons, respectively, and a $\tau_{\text{had}}\tau_{\text{had}}$ trigger with p_{T} thresholds of 38 GeV for each hadronically decaying τ lepton.

With two τ leptons in the final state, it is not possible to infer the neutrino momenta from the reconstructed $E_{\text{T}}^{\text{miss}}$ vector to estimate the $\tau\tau$ invariant mass difficult. Two approaches are used. The first method used is the Missing Mass Calculator (MMC) [68]. This algorithm assumes that the missing transverse momentum is due entirely to the neutrinos, and performs a scan over the angles between the neutrinos and the visible τ lepton decay products. The MMC mass, $m_{\tau\tau}^{\text{MMC}}$, is defined as the most likely value chosen by weighting each solution according to probability density functions that are derived from simulated τ lepton decays. As an example, the MMC resolution[4], assuming a Higgs boson with mass $m_{\text{A}} = 150$ GeV, is about 30% for $\tau_{\text{e}}\tau_{\mu}$ events. The resolution is about 20% for $\tau_{\text{lep}}\tau_{\text{had}}$ events ($\tau_{\text{lep}} = \tau_{\text{e}}$ or τ_{μ}) for Higgs bosons with a mass of either $m_{\text{A}} = 150$ or 350 GeV. The second method uses the $\tau\tau$ total

[4]The resolution of the mass reconstruction is estimated by dividing the root mean square of the mass distribution by its mean.

transverse mass, defined as:

$$m_{\mathrm{T}}^{\mathrm{total}} = \sqrt{m_{\mathrm{T}}^2(\tau_1,\tau_2) + m_{\mathrm{T}}^2(\tau_1, E_{\mathrm{T}}^{\mathrm{miss}}) + m_{\mathrm{T}}^2(\tau_2, E_{\mathrm{T}}^{\mathrm{miss}})} \ ,$$

where the transverse mass, m_{T}, between two objects with transverse momenta $p_{\mathrm{T}1}$ and $p_{\mathrm{T}2}$ and relative angle $\Delta\phi$ is given by

$$m_{\mathrm{T}} = \sqrt{2p_{\mathrm{T}1}p_{\mathrm{T}2}(1-\cos\Delta\phi)} \ .$$

As an example, the $m_{\mathrm{T}}^{\mathrm{total}}$ mass resolution assuming a Higgs boson with mass $m_\phi = 350$ GeV for $\tau_{\mathrm{had}}\tau_{\mathrm{had}}$ events is approximately 30%. While the MMC exhibits a better $\tau\tau$ mass resolution for signal events, multi-jet background events tend to be reconstructed at lower masses with $m_{\mathrm{T}}^{\mathrm{total}}$, leading to an overall better signal to background discrimination for topologies dominated by multi-jet background.

5.1 The $\mathrm{h/H/A} \to \tau_{\mathrm{e}}\tau_{\mu}$ channel

Events in the $h/H/A \to \tau_{\mathrm{e}}\tau_{\mu}$ channel are selected using either single electron or electron-muon triggers. The data sample corresponds to an integrated luminosity of 20.3 fb^{-1}. Exactly one isolated electron and one isolated muon of opposite charge are required, with lepton p_{T} thresholds of 15 GeV for electrons and 10 GeV for muons. Electrons with p_{T} in the range 15–25 GeV are from events selected by the electron-muon trigger, whereas for $p_{\mathrm{T}} > 25$ GeV are selected by the single electron trigger. Events containing hadronically decaying τ leptons, passing the "loose" τ_{had} identification criterion, are vetoed.

To increase the sensitivity of this channel, the events are split into two categories based on the presence ("tag category") or absence ("veto category") of a b-tagged jet. The tag category requires exactly one jet passing the b-jet identification criterion. In addition, a number of kinematic requirements are imposed to reduce the background from top quark decays. The azimuthal angle between the electron and the muon, $\Delta\phi(e,\mu)$, must be greater than 2. The sum of the cosines of the azimuthal angles between the leptons and the $E_{\mathrm{T}}^{\mathrm{miss}}$, $\Sigma\cos\Delta\phi \equiv \cos(\phi(e) - \phi(E_{\mathrm{T}}^{\mathrm{miss}})) + \cos(\phi(\mu) - \phi(E_{\mathrm{T}}^{\mathrm{miss}}))$, must be greater than -0.2. The scalar sum of the p_{T} of jets with $p_{\mathrm{T}} > 30$ GeV must be less than 100 GeV. Finally, the scalar sum of the p_{T} of the leptons and the $E_{\mathrm{T}}^{\mathrm{miss}}$ must be below 125 GeV. The veto category is defined by requiring that no jet passes the b-jet identification criterion. Because the top quark background is smaller in this category, the imposed kinematic selection requirements, $\Delta\phi(e,\mu) > 1.6$ and $\Sigma\cos\Delta\phi > -0.4$, are looser than in the tag category.

The most important background processes in this channel are Z/γ^*+jets, $t\bar{t}$, and multi-jet production. The $Z/\gamma^* \to \tau\tau$ background is estimated using the τ-embedded $Z/\gamma^* \to \mu^+\mu^-$ sample outlined in Section 3. It is normalized using the NNLO Z/γ^* + jets cross section calculated with FEWZ [69] and an estimate of the trigger and lepton η, p_{T} and identification efficiency from simulation. The $t\bar{t}$ background is estimated from simulation with the normalization taken from a data control region enriched in $t\bar{t}$ events. W+jet background where one of the leptons results from a misidentified jet is estimated using simulation. Smaller backgrounds from single top, and diboson production are also estimated from simulation.

The multi-jet background is estimated from data using a two-dimensional sideband method. The event sample is split into four regions according to the charge product of the $e\mu$ pair and the isolation requirements on the electron and muon. Whereas region A (B) contains events where both leptons pass the isolation requirements and are of opposite (same) charge, region C (D) similarly contains events where both leptons fail the isolation requirements. This way, A is the signal region, whereas B, C, and D are control regions. Event contributions to the B, C and D control regions from processes other than multi-jet production are estimated using simulation and subtracted. The final prediction for the multi-jet contribution to the signal region, A, is given by the background-subtracted data in region B, scaled by the opposite-sign to same-sign ratio measured in regions C and D, $r_{C/D} \equiv n_C/n_D$. Systematic uncertainties for the prediction are estimated from the stability of $r_{C/D}$ under variations of the lepton isolation cut value.

	Tag category		Veto category	
Signal (m_A = 150 GeV, $\tan\beta$ = 20)	140	±30	2020	±130
$Z/\gamma^* \to \tau\tau$+jets	420	±30	55000	±4000
Multi-jet	100	±21	4200	±700
$t\bar{t}$ and Single Top	420	±50	2700	±400
Others	26	±7	4010	±280
Total background	970	±60	66000	±4000
Data	904		65917	

Table 1: Number of events observed for the $h/H/A \to \tau_e\tau_\mu$ channel and the predicted background and signal. The predicted signal event yields correspond to the parameter choice m_A = 150 GeV and $\tan\beta$ = 20. The row labeled "Others" includes events from diboson production, $Z/\gamma^* \to ee/\mu\mu$ and W+jets production. Combined statistical and systematic uncertainties are quoted. The signal prediction does not include the uncertainty due to the cross section calculation.

Table 1 shows the number of observed $\tau_e\tau_\mu$ events, the prediction of the background and the signal prediction for the MSSM $m_h^{\max}$ scenario parameter choice m_A = 150 GeV, $\tan\beta$ = 20. The table quotes also the total combined statistical and systematic uncertainties in the predictions. The observed event yields are compatible with the expected yields from SM processes. The MMC mass is used as the discriminating variable in this channel, and is shown in Figure 2 for the tag and veto categories separately.

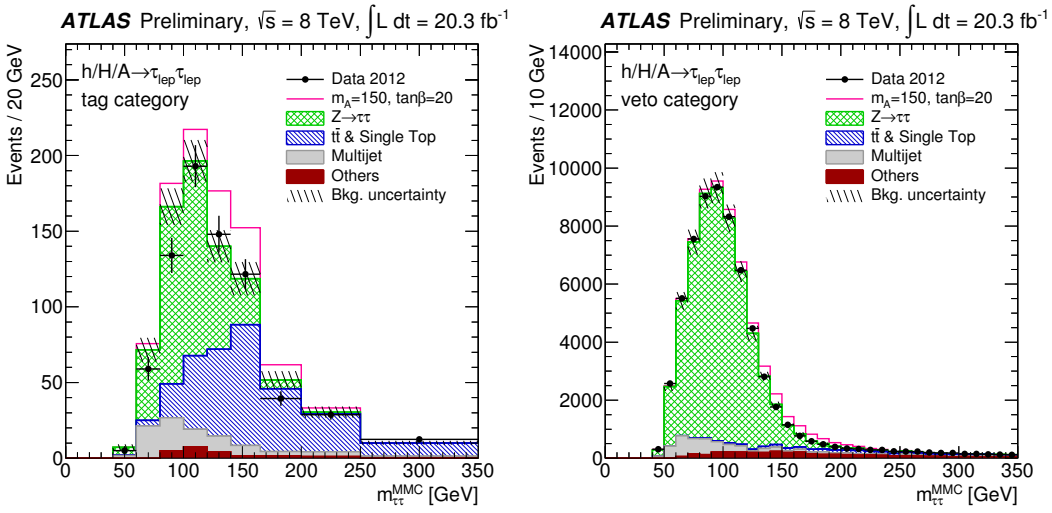

Figure 2: MMC mass distributions for the $h/H/A \to \tau_e\tau_\mu$ channel. The MMC mass is shown for the tag (left panel) and the veto categories (right panel). The data are compared to the background expectation and a hypothetical MSSM signal ($m_A = 150$ GeV and $\tan\beta = 20$). The contributions of the diboson, $Z/\gamma^* \to ee/\mu\mu$, and W+jets background processes are combined and labelled "Others". The background uncertainty includes statistical and systematic uncertainties.

5.2 The h/H/A $\rightarrow \tau_{\text{lep}}\tau_{\text{had}}$ channel

Events in the $h/H/A \rightarrow \tau_{\text{lep}}\tau_{\text{had}}$ channel are selected using single electron or single muon triggers. The data sample corresponds to an integrated luminosity of 20.3 fb^{-1}. Events are required to contain an electron or a muon with $p_{\text{T}} > 26$ GeV and an oppositely-charged τ_{had} with $p_{\text{T}} > 20$ GeV satisfying the "medium" τ_{had} identification criterion. Events must not contain additional electrons or muons.

The event selection is optimised separately for low and high mass Higgs bosons in order to exploit differences in kinematics and background composition.

The low mass selection targets the parameter space with $m_{\text{A}} < 200$ GeV. It includes two orthogonal categories: the tag category and the veto category. In the tag category there must be at least one jet tagged as a b-jet. No other jet than the leading b-jet must have a p_{T} exceeding 30 GeV, and the transverse mass between the lepton and the $E_{\text{T}}^{\text{miss}}$ is required to not exceed 45 GeV. These requirements serve to reduce the otherwise dominant $t\bar{t}$ background. In the veto category there must be no jet tagged as b-jet. Two additional selection requirements are applied to reduce the W + jets background. First, the transverse mass between the lepton and the $E_{\text{T}}^{\text{miss}}$ must be below 60 GeV. Secondly, the sum of the azimuthal angles between the τ_{had}–$E_{\text{T}}^{\text{miss}}$ pair and the lepton–$E_{\text{T}}^{\text{miss}}$ pair, $\Sigma\Delta\phi \equiv \Delta\phi(\tau_{\text{had}}, E_{\text{T}}^{\text{miss}}) + \Delta\phi(\tau_{\text{lep}}, E_{\text{T}}^{\text{miss}})$, must have a value less than 3.3. Finally, in the $\tau_\mu\tau_{\text{had}}$ channel of the veto category, dedicated requirements based on kinematic and shower shape properties of the tau candidate are applied to reduce the number of muons faking hadronic tau decays.

The high mass selection targets $m_{\text{A}} \geq 200$ GeV. It is required that $\Sigma\Delta\phi < 3.3$, in order to reduce the W+jets background. The hadronic and leptonic tau decays are requested to be back-to-back: $\Delta\phi(\tau_{\text{lep}}, \tau_{\text{had}}) > 2.4$. In addition, the transverse momentum difference between the τ_{had} and the lepton, $\Delta p_{\text{T}} \equiv p_{\text{T}}(\tau_{\text{had}}) - p_{\text{T}}(\text{lepton})$, must be above 45 GeV. This requirement takes advantage of the fact that a τ_{had} tends to have a higher visible transverse momentum than a τ_{lep} due to the presence of more neutrinos in the latter decay.

In the low-mass categories, the electron and muon channels are treated separately and combined statistically. For the high-mass category, they are treated as a single channel to improve the statistical robustness.

The most important SM background processes in this channel are Z/γ^* + jets, W + jets, multi-jet production, top (including both $t\bar{t}$ and single top) and diboson production. The τ-embedded $Z/\gamma^* \rightarrow \mu^+\mu^-$ sample is used to estimate the $Z/\gamma^* \rightarrow \tau\tau$ background. It is normalised in the same way as in the $\tau_{\text{lep}}\tau_{\text{lep}}$ channel. The rate at which electrons are misidentified as τ_{had}, important mostly for $Z \rightarrow ee$ decays, has been estimated from data [66]. The contribution of diboson processes is small and estimated from simulation. Events originating from W+jets, $Z(\rightarrow \ell\ell)$+ jets ($\ell = e, \mu$), $t\bar{t}$ and single top production, in which a jet is misreconstructed as τ_{had}, are estimated from simulated samples with normalisation defined by comparing event yields in background-dominated control regions in data. Separate regions are defined for the low-mass tag, low-mass veto, and high-mass categories. Systematic uncertainties are derived using alternative definitions for the control regions. The multi-jet background is estimated with a two-dimensional sideband method, similar to the one employed for the $\tau_{\text{e}}\tau_\mu$ channel, using the lepton (e or μ) - τ_{had} charge product and lepton isolation. The systematic uncertainty on the predicted event yield is estimated by varying the definitions of the regions used, and by testing the stability of the $r_{C/D}$ ratio across the $m_{\tau\tau}^{\text{MMC}}$ range.

Table 2 shows the number of observed $\tau_{\text{lep}}\tau_{\text{had}}$ events, the prediction of the background, and the signal prediction for the MSSM m_h^{max} scenario parameter choices $m_A = 150$ GeV, $\tan\beta = 20$ for the low mass categories and $m_A = 350$ GeV, $\tan\beta = 30$ for the high mass category. The table quotes also the total combined statistical and systematic uncertainties in the predictions. The observed event yields are compatible with the expected yields from Standard Model processes within the uncertainties. The MMC mass is used as the final mass discriminant in this channel and is shown in Figures 3 and 4 for the low and high mass categories, respectively.

Low mass categories

	Tag category				Veto category			
	e channel		μ channel		e channel		μ channel	
Signal (m_A = 150 GeV, $\tan\beta$ = 20)	190	±40	190	±40	1870	±90	1840	±90
$Z \to \tau\tau$+jets	400	±40	430	±40	31700	±2800	38400	±3300
$Z \to \ell\ell$+jets ($\ell = e, \mu$)	70	±24	33	±14	6000	±900	2900	±500
W+jets	160	±40	190	±60	9100	±1300	9800	±1400
Multi-jet	185	±35	66	±31	11700	±500	3100	±400
$t\bar{t}$ and Single Top	230	±40	236	±34	530	±90	500	±100
Diboson	9.1	±2.3	10.0	±2.5	470	±40	470	±40
Total background	1060	±80	960	±90	59400	±3300	55000	±4000
Data	1067		947		60351		54776	

High mass category

Signal (m_A = 350 GeV, $\tan\beta$ = 30)	315	±18
$Z \to \tau\tau$+jets	410	±50
$Z \to \ell\ell$+jets ($\ell = e, \mu$)	35	±7
W+jets	210	±40
Multi-jet	57	±20
$t\bar{t}$ and Single Top	184	±26
Diboson	30	±5
Total background	930	±70
Data	920	

Table 2: Number of events observed for the $h/H/A \to \tau_{\text{lep}}\tau_{\text{had}}$ channel and the predicted background and signal. The predicted signal event yields correspond to the parameter choice m_{A} = 150 GeV, $\tan\beta$ = 20 for the low mass categories and m_{A} = 350 GeV, $\tan\beta$ = 30 for the high mass category. Combined statistical and systematic uncertainties are quoted. The signal prediction does not include the uncertainty due to the cross section calculation.

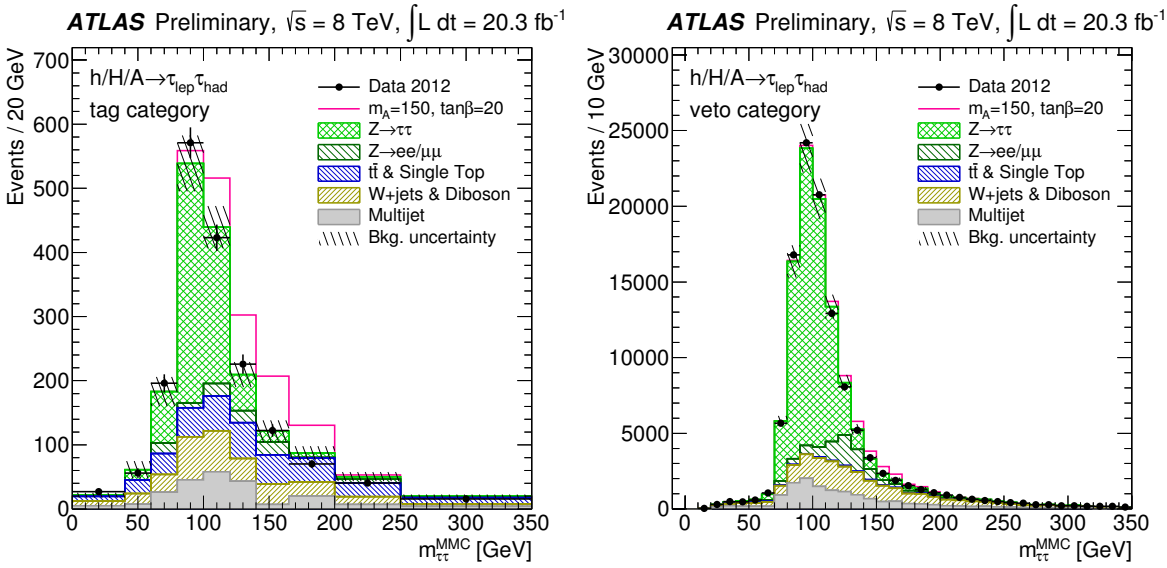

Figure 3: MMC mass distributions for the low-mass categories of the $h/H/A \rightarrow \tau_{\text{lep}}\tau_{\text{had}}$ channel. Tag (left panel) and veto (right panel) categories are shown for the combined $\tau_{\text{e}}\tau_{\text{had}}$ and $\tau_{\mu}\tau_{\text{had}}$ final states. The data are compared to the background expectation and a hypothetical MSSM signal ($m_{\text{A}} = 150$ GeV and $\tan\beta = 20$). The background uncertainty includes statistical and systematic uncertainties.

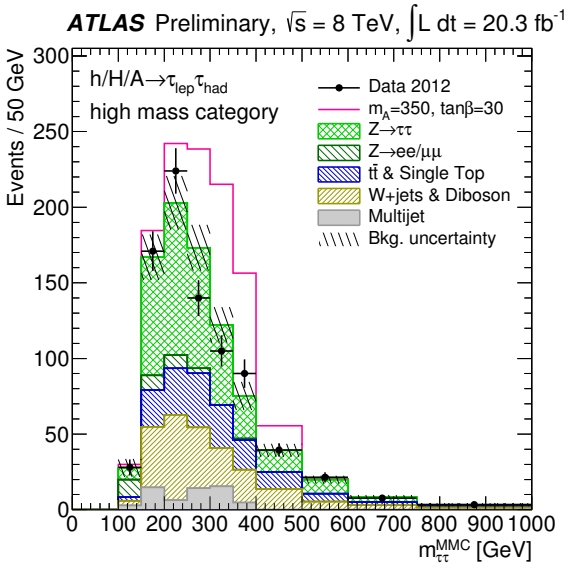

Figure 4: MMC mass distributions for the high-mass category of the $h/H/A \rightarrow \tau_{\text{lep}}\tau_{\text{had}}$ channel shown for the combined $\tau_{\text{e}}\tau_{\text{had}}$ and $\tau_{\mu}\tau_{\text{had}}$ final states. The data are compared to the background expectation and a hypothetical MSSM signal ($m_{\text{A}} = 350$ GeV and $\tan\beta = 30$). The background uncertainty include statistical and systematic uncertainties.

5.3 The h/H/A $\rightarrow \tau_{\text{had}}\tau_{\text{had}}$ channel

Events in the $h/H/A \rightarrow \tau_{\text{had}}\tau_{\text{had}}$ channel are selected using either a single τ_{had} trigger or a $\tau_{\text{had}}\tau_{\text{had}}$ trigger. The data sample corresponds to an integrated luminosity of 19.5 fb^{-1}. Events are required to contain at least two τ_{had}, identified using the "loose" identification criterion. If more than two τ_{had} are present, the two with the highest p_{T} values are considered. Events containing an electron or muon are rejected to ensure orthogonality with the other channels. The two τ_{had} are required to have $p_{\text{T}} >$ 50 GeV, have opposite electric charges, and to be back-to-back in the azimuthal plane ($\Delta\phi > 2.7$). Two event categories are defined as follows. The single-τ_{had} trigger category (STT category) includes the events selected by the single τ_{had} trigger that contain at least one τ_{had} with $p_{\text{T}} > 150$ GeV. The $\tau_{\text{had}}\tau_{\text{had}}$ trigger category (DTT category) includes the events selected by the $\tau_{\text{had}}\tau_{\text{had}}$ trigger, with the leading τ_{had} required to have pT less than 150 GeV, to ensure orthogonality with the STT category, and with both taus passing the "medium" identification criterion. In addition, events in the DTT category are required to have $E_{\text{T}}^{\text{miss}} > 10$ GeV, and the scalar sum of transverse energy of all deposits in the calorimeter to be greater than 160 GeV.

The dominant background in this channel is multi-jet production and for this reason the $m_{\text{T}}^{\text{total}}$ is used as a final discriminant. Other processes include Z/γ^* + jets, W + jets, $t\bar{t}$ and diboson.

The multi-jet background is estimated separately for the STT and DTT categories. A control region is defined in the STT category by requiring the next-to-highest-p_{T} τ_{had} to fail the "loose" τ_{had} identification criterion, thus obtaining a high purity sample of multi-jet events. The number of multi-jet events in the signal region is then estimated by extrapolating from this control region. The extrapolation is performed by measuring the ratio between the number of jets passing and failing the same τ_{had} identification criterion in a pure sample of di-jet events. An estimate for the systematic uncertainty of the method is obtained based on the charge product of the two jets in this control sample. The uncertainty is in the range 2–30% depending on the jet p_{T} and number of associated tracks. A two-dimensional sideband method is used in the DTT category by defining four regions based on the charge product of the two τ_{had} and the $E_{\text{T}}^{\text{miss}} > 10$ GeV requirement. A systematic uncertainty is derived by measuring the variation of the ratio of opposite-sign over same-sign $\tau_{\text{had}}\tau_{\text{had}}$ pairs for different sideband region definition, as well as across the $m_{\text{T}}^{\text{total}}$ range, and amounts to 5%.

The remaining backgrounds are modelled using simulation. Non-multi-jet processes with jets faking taus are dominated by $W(\rightarrow \tau\nu)$+jets. Their contribution is estimated by simulation, which is corrected using the efficiency of a jet to be misidentified as a τ_{had} measured in a control region in data. Z/γ^* + jets background is also estimated using simulation. Due to the low statistics after the p_{T} thresholds of the tau trigger requirements, the tau-embedded $Z \rightarrow \mu\mu$ sample is not used.

Table 3 shows the number of observed $\tau_{\text{had}}\tau_{\text{had}}$ events, the prediction of the background and the signal prediction for the MSSM m_h^{max} scenario parameter choice $m_A = 350$ GeV, $\tan\beta = 30$. The table quotes also the total combined statistical and systematic uncertainties in the predictions. The observed event yields are compatible with the expected yields from SM processes within the uncertainties. The distributions of the total transverse mass are shown in Figure 5 for the STT and the DTT categories separately.

	Single-τ_{had} trigger (STT) category		$\tau_{\text{had}}\tau_{\text{had}}$ trigger (DTT) category	
Signal (m_A = 350 GeV, $\tan\beta$ = 30)	177	±35	340	±50
Multi-jet	216	±25	6800	±400
$Z/\gamma^* \to \tau\tau$	113	±18	750	±210
$W(\to \tau\nu)$+jets	34	±8	400	±100
$t\bar{t}$ and Single Top	10	±4	76	±26
Others	0.50	±0.20	3.4	±0.8
Total background	370	±30	8000	±500
Data	373		8225	

Table 3: Number of events observed for the $h/H/A \to \tau_{\text{had}}\tau_{\text{had}}$ channel and the predicted background and signal. The predicted signal event yields correspond to the parameter choice m_{A} = 350 GeV, $\tan\beta$ = 30. The row labeled "Others" include events from diboson production, $Z \to ll$ and $W \to l\nu$ with $l = e, \mu$. Combined statistical and systematic uncertainties are quoted. The signal prediction does not include the uncertainty due to the cross section calculation.

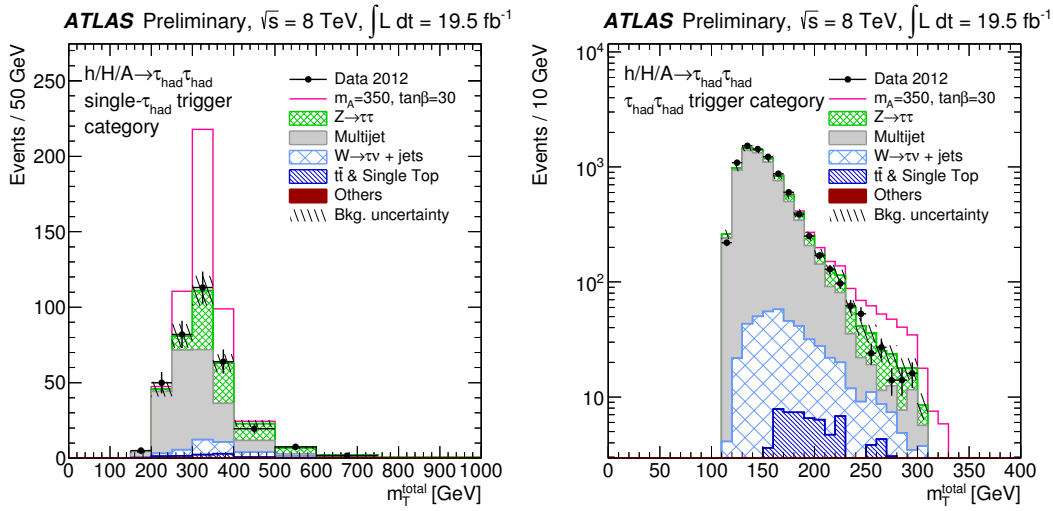

Figure 5: Total transverse mass distributions for STT (left panel) and DTT (right panel) categories of the $h/H/A \to \tau_{\text{had}}\tau_{\text{had}}$ channel. The data are compared to the background expectation and a hypothetical MSSM signal (m_{A} = 350 GeV and $\tan\beta$ = 30). The background labeled "Others" includes events from diboson production, $Z \to ll$ and $W \to l\nu$ with $l = e, \mu$. The background uncertainty includes statistical and systematic uncertainties.

6 Systematic Uncertainties

The event yields for several of the backgrounds in this search have been estimated using control samples in data as described in Section 5 and their associated uncertainties are discussed there. In this section, the remaining uncertainties are discussed and the overall effect of the systematic uncertainties is presented.

Signal cross section uncertainties are taken from the study in Ref. [70]. Typical uncertainty values are in the range 10–15% for gluon-fusion and 15–20% for b-associated production.

The uncertainty on the signal acceptance from the parameters used in the event generation of signal and background samples is also considered. This is done by evaluating the change in acceptance after varying the relevant scale parameters, parton distribution function choices, and if applicable, conditions for the matching of the partons used in the fixed order calculation and the parton shower. The uncertainty on the signal acceptance is largest in the tag category for b-associated production where it is about 13%.

Uncertainties for single boson and diboson production cross sections have been estimated for missing higher order corrections, parton density functions and the value of the strong coupling constant, and have been considered wherever applicable. Acceptance uncertainties for these background processes have been estimated in the same way as for signal. The most important theoretical uncertainties on the background are the Z+jets cross section and acceptance that affect the normalisation by about 7%.

The uncertainty on the integrated luminosity is 2.8%. It is derived, following the same methodology as that detailed in Ref. [71], from a preliminary calibration of the luminosity scale derived from beam-separation scans performed in November 2012.

The single and double τ_{had} trigger efficiencies are studied in $Z \to \tau\tau$ events. Their uncertainties are in the range 3–25% depending on the pseudorapidity, p_{T} and the number of the associated tracks of the hadronic tau decay as well as the data taking period and they are estimated with a method similar to Ref. [72] updated for the 2012 data taking conditions.

The τ_{had} identification efficiency is measured using $Z \to \tau\tau$ events. The uncertainty is in the range 3–10% depending on the pseudorapidity and the number of tracks matched to the τ lepton [66]. Extrapolated uncertainties are used for τ_{had} candidates with transverse momenta above those accessible in $Z \to \tau\tau$ events.

The τ_{had} energy scale uncertainty is estimated by propagating the single particle response to the individual τ_{had} decay products (neutral and charged pions). This uncertainty is in the range 2–4% [73] depending on p_{T}, pseudorapidity and the number of associated tracks.

The jet energy scale (JES) and resolution uncertainties are described in Refs. [63] and [74]. The JES is established by exploiting the p_{T} balance between a jet and a reference object such as a Z boson or a photon. The uncertainty ranges between 3% and 7% depending on the p_{T} and pseudorapidity.

The b-jet identification efficiency uncertainty ranges from 2% to 8% depending on the jet p_{T}. The estimation of this uncertainty is based on a study that uses $t\bar{t}$ events in data [64].

The $E_{\text{T}}^{\text{miss}}$ uncertainties are derived by propagating all reconstructed object energy scale uncertainties. Additionally, the scale for energy outside reconstructed objects and the resolution uncertainties are considered [75].

Electron and muon reconstruction, identification, isolation and trigger efficiency uncertainties have been estimated from data [60, 76]. Electron energy scale and resolution and muon momentum scale and resolution uncertainties are also estimated from data and taken into account [60, 77].

Systematic uncertainties associated with the τ-embedded $Z/\gamma^* \to \mu^+\mu^-$+jets data event sample have been investigated [28, 58]. Two are found to be the most significant: the uncertainty due to the muon selection, which is estimated by varying the muon isolation requirement used in selecting the $Z/\gamma^* \to \mu^+\mu^-$+jets events, and the uncertainty from the subtraction of the calorimeter cell energy associated with the muon. The $\mu^+\mu^-$ sample used for embedding is expected to have a sizable contamination due to $t\bar{t}$ events in the high MMC mass region, particularly after the $\tau_{\text{lep}}\tau_{\text{had}}$ tag category selection. Therefore

an additional uncertainty of 50% on the $Z \rightarrow \tau\tau$ background is added for the $\tau_{\text{lep}}\tau_{\text{had}}$ tag cateogry for $m_{\tau\tau}^{\text{MMC}} > 135$ GeV, and a 20% uncertainty for the $\tau_{\text{lep}}\tau_{\text{had}}$ high mass category for $m_{\tau\tau}^{\text{MMC}} > 400$ GeV.

The relative effect of each of the systematic uncertainties can be seen by their influence on the signal strength parameter, μ, defined as the ratio of the fitted to the assumed signal cross section times branching ratio (see also Section 7). In the low mass analysis the dominant uncertainties on μ arise from τ_{had} energy scale, jet energy scale, electron and muon identification, Z+jets normalisation and lepton-to-tau fake rate. In the high mass analyses they are due to the τ_{had} energy scale, the multi-jet estimation, the τ_{had} identification and the τ_{had} trigger.

7 Results

The results from the channels studied in this search are combined to improve the sensitivity to the MSSM Higgs boson production. Each of the channels used here has been optimized for specific Higgs boson mass regimes. In particular, the $\tau_{\text{e}}\tau_{\mu}$ channel, the $\tau_{\text{lep}}\tau_{\text{had}}$ tag category, and the $\tau_{\text{lep}}\tau_{\text{had}}$ veto category are used for the range $90 \leq m_A < 200$ GeV. The $\tau_{\text{lep}}\tau_{\text{had}}$ high mass category and the $\tau_{\text{had}}\tau_{\text{had}}$ channel are used for $m_A \geq 200$ GeV.

The parameter of interest in this search is the signal strength, μ defined by the ratio of the fitted signal cross section times branching ratio to the signal cross section times branching ratio predicted by the particular MSSM signal assumption. The value $\mu = 0$ corresponds to the absence of signal, whereas the value $\mu = 1$ suggests signal presence as predicted by the theoretical model under study. The statistical analysis of the data employs a binned likelihood function constructed as the product of Poisson probability terms as an estimator of μ. Signal and background predictions depend on uncertainties that are parameterised as nuisance parameters and are constrained using Gaussian functions. The binned likelihood function is constructed in bins of the MMC mass for the $\tau_{\text{e}}\tau_{\mu}$ and the $\tau_{\text{lep}}\tau_{\text{had}}$ channels and in bins of total transverse mass for the $\tau_{\text{had}}\tau_{\text{had}}$ channel.

Since the data are in good agreement with the predicted background yields, exclusion limits are calculated. The significance of any small observed excess in data is evaluated by quoting p-values. Exclusion limits use the modified frequentist method known as CL_s [78]. Both exclusion limits and p-values are calculated using the asymptotic approximation [79]. The test statistic used for the exclusion limits derivation is the $\tilde{q}_{\mu}$ test statistic and for the p-values the q_0 test statistic[5] [79].

The lowest local p-value for the statistical combination corresponds to 0.20, or 0.8 σ in terms of Gaussian standard deviations, at $m_{\phi} = 200$ GeV. For the individual channels, the lowest local p-value in $\tau_{\text{had}}\tau_{\text{had}}$ is 0.10 (or 1.3 σ) at $m_{\phi} = 250$ GeV and for the $\tau_{\text{lep}}\tau_{\text{had}}$ 0.10 (or 1.3 σ) at $m_{\phi} = 90$ GeV. In the $\tau_{\text{lep}}\tau_{\text{lep}}$ channel there is no excess in the mass region used for the combination ($90 \leq m_{\phi} < 200$ GeV).

Expected and observed upper limits for the statistical combination of all channels are shown in Figure 6(a) for the MSSM m_h^{max} scenario with $M_{\text{SUSY}} = 1$ TeV [32,33]. In this figure, the theoretical MSSM Higgs cross section uncertainties are not included in the reported result, but their impact is shown separately, by recalculating the upper limits again after considering the relevant $\pm 1\sigma$ variations. The upper

[5]The definition of the test statistics used in this search is the following:

$$\tilde{q}_{\mu} = \begin{cases} -2\ln(\mathcal{L}(\mu,\hat{\theta})/\mathcal{L}(0,\hat{\hat{\theta}})) & \text{if } \hat{\mu} < 0 \\ -2\ln(\mathcal{L}(\mu,\hat{\theta})/\mathcal{L}(\hat{\mu},\hat{\theta})) & \text{if } 0 \leq \hat{\mu} \leq \mu \\ 0 & \text{if } \hat{\mu} > \mu \end{cases}$$

and

$$q_0 = \begin{cases} -2\ln(\mathcal{L}(0,\hat{\hat{\theta}})/\mathcal{L}(\hat{\mu},\hat{\theta})) & \text{if } \hat{\mu} \geq 0 \\ 0 & \text{if } \hat{\mu} < 0 \end{cases}$$

where $\mathcal{L}(\mu,\theta)$ denotes the binned likelihood function, μ is the parameter of interest (i.e. the signal strength parameter), and θ denotes the nuisance parameters. The pair $(\hat{\mu},\hat{\theta})$ corresponds to the global maximum of the likelihood, whereas $(x,\hat{\hat{\theta}})$ corresponds to a conditional maximum in which μ is fixed to a given value x.

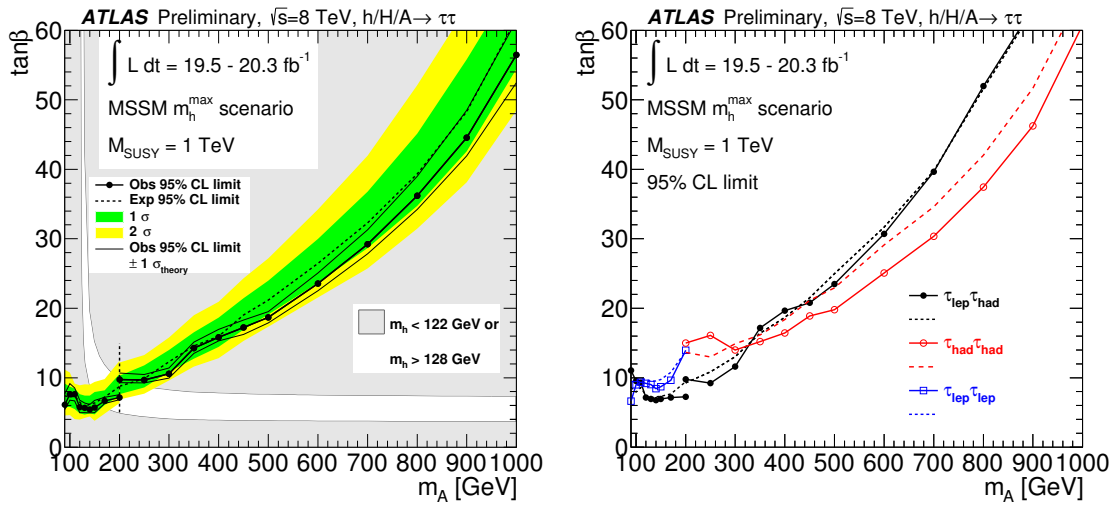

(a) (b)

Figure 6: Expected (dashed line) and observed (solid line with markers) 95% CL upper limits on $\tan\beta$ as a function of m_{A}. Values of $\tan\beta$ above the lines are excluded. The upper limits are shown in (a) for the statistical combination of all channels and in (b) for each channel separately. The vertical dashed line at 200 GeV indicates the transition point between low and high mass categories. The $m_{\mathrm{A}} - \tan\beta$ plane region which is incompatible with a light, CP-even Higgs boson with mass in the range 122–128 GeV is shown as a gray area in (a). For more information, see text.

limits for each channel separately for comparison is shown for the same configuration in Figure 6(b). The best $\tan\beta$ constraint for the combined search excludes $\tan\beta > 5.4$ for $m_A = 140$ GeV. For high mass $\tan\beta > 36$ is excluded for $m_A = 800$ GeV. Figure 6(a) shows also the region in the MSSM m_h^{max} parameter space that is not compatible with a light CP-even Higgs boson with a mass in the range 122–128 GeV within this model. From this region is is concluded that if the light CP-even Higgs boson of the MSSM is identified with the particle discovered at the LHC, then for this particular MSSM scenario $m_A < 160$ GeV is excluded for all $\tan\beta$ values and $\tan\beta > 10$ is excluded for all m_A values.

The outcome of the search is further interpreted in the case of a single scalar boson ϕ with narrow width relative to the experimental mass resolution produced in either the gluon-fusion or b-associated production mode and decaying to $\tau\tau$. Figure 7 shows 95% CL upper limits on the cross section times the $\tau\tau$ branching fraction based on this interpretation. The exclusion limits for the production cross section times the branching fraction for a Higgs boson decaying to $\tau\tau$ are shown as a function of the Higgs boson mass. The excluded cross section times branching fraction values range from $\sigma \times BR > 29$ pb at $m_\phi = 90$ GeV to $\sigma \times BR > 7.4$ pb at $m_\phi = 1000$ GeV for a Higgs boson produced via gluon-fusion. The exclusion range for the b-associated production mechanism is from $\sigma \times BR > 6.4$ pb at $m_\phi = 90$ GeV to $\sigma \times BR > 7.2$ fb at $m_\phi = 1000$ GeV.

8 Conclusions

A search is presented for the neutral Higgs bosons of the Minimal Supersymmetric Standard Model in proton–proton collisions at the centre-of-mass energy of 8 TeV with the ATLAS experiment at the LHC. The integrated luminosity used in the search is 19.5–20.3 fb^{-1}. The search uses the $\tau\tau$ final state. In particular, the following cases have been considered: one τ lepton decays to an electron and the other to a muon ($\tau_{\mathrm{e}}\tau_{\mu}$), one τ lepton decays to an electron or muon and the other hadronically ($\tau_{\mathrm{lep}}\tau_{\mathrm{had}}$) and finally

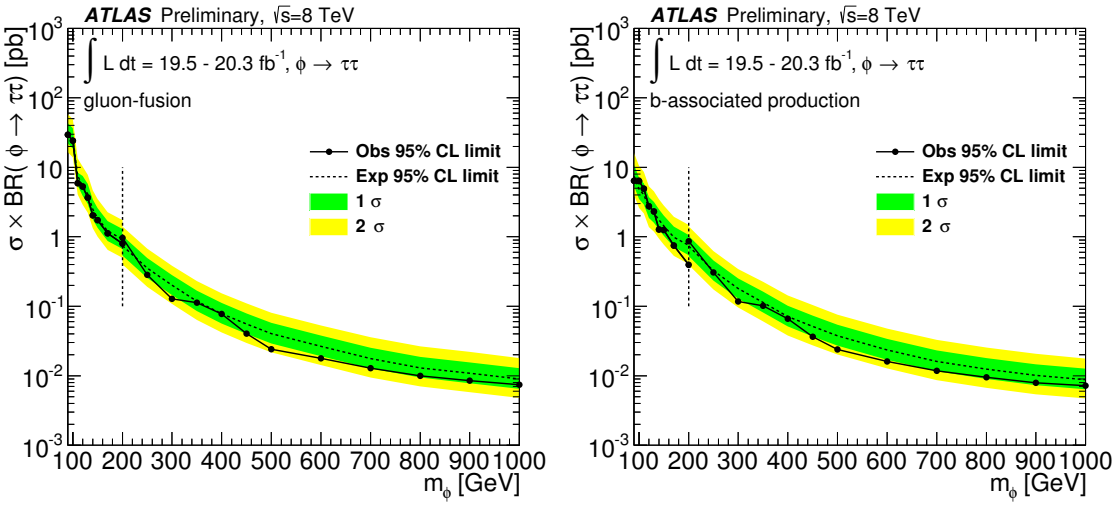

(a) (b)

Figure 7: Expected (dashed bold line) and observed (solid bold line) 95% CL upper limits on the cross section for gluon-fusion (a) and b-associated Higgs boson production (b) times the branching ratio into τ pairs.

both τ leptons decay hadronically ($\tau_{\text{had}}\tau_{\text{had}}$). The sensitivity is improved by performing a categorization based on Higgs boson mass and production mechanisms. The search finds no indication of an excess over the expected background in the channels considered and 95% CL limits are set, which provide tight constraints to the MSSM parameter space. In particular, in the context of the MSSM m_h^{max} scenario the lowest $\tan\beta$ constrain excludes $\tan\beta > 5.4$ for $m_A = 140$ GeV. Upper limits for the production cross section times $\tau\tau$ branching fraction of a scalar boson versus its mass, depending on the production mode, are also presented. The excluded cross section times $\tau\tau$ branching fraction range from about 30 pb to about 7 fb depending on the Higgs boson mass and the production mechanism.

Acknowledgements

We thank CERN for the very successful operation of the LHC, as well as the support staff from our institutions without whom ATLAS could not be operated efficiently.

We acknowledge the support of ANPCyT, Argentina; YerPhI, Armenia; ARC, Australia; BMWF and FWF, Austria; ANAS, Azerbaijan; SSTC, Belarus; CNPq and FAPESP, Brazil; NSERC, NRC and CFI, Canada; CERN; CONICYT, Chile; CAS, MOST and NSFC, China; COLCIENCIAS, Colombia; MSMT CR, MPO CR and VSC CR, Czech Republic; DNRF, DNSRC and Lundbeck Foundation, Denmark; EPLANET, ERC and NSRF, European Union; IN2P3-CNRS, CEA-DSM/IRFU, France; GNSF, Georgia; BMBF, DFG, HGF, MPG and AvH Foundation, Germany; GSRT and NSRF, Greece; ISF, MINERVA, GIF, I-CORE and Benoziyo Center, Israel; INFN, Italy; MEXT and JSPS, Japan; CNRST, Morocco; FOM and NWO, Netherlands; BRF and RCN, Norway; MNiSW and NCN, Poland; GRICES and FCT, Portugal; MNE/IFA, Romania; MES of Russia and ROSATOM, Russian Federation; JINR; MSTD, Serbia; MSSR, Slovakia; ARRS and MIZŠ, Slovenia; DST/NRF, South Africa; MINECO, Spain; SRC and Wallenberg Foundation, Sweden; SER, SNSF and Cantons of Bern and Geneva, Switzerland; NSC, Taiwan; TAEK, Turkey; STFC, the Royal Society and Leverhulme Trust, United Kingdom; DOE and NSF, United States of America.

The crucial computing support from all WLCG partners is acknowledged gratefully, in particular

from CERN and the ATLAS Tier-1 facilities at TRIUMF (Canada), NDGF (Denmark, Norway, Sweden), CC-IN2P3 (France), KIT/GridKA (Germany), INFN-CNAF (Italy), NL-T1 (Netherlands), PIC (Spain), ASGC (Taiwan), RAL (UK) and BNL (USA) and in the Tier-2 facilities worldwide.

References

[1] ATLAS Collaboration, *Observation of a new particle in the search for the Standard Model Higgs boson with the ATLAS detector at the LHC*, Phys. Lett. **B716** (2012) 1–29, arXiv:1207.7214 [hep-ex].

[2] CMS Collaboration, *Observation of a new boson at a mass of 125 GeV with the CMS experiment at the LHC*, Phys. Lett. **B716** (2012) 30–61, arXiv:1207.7235 [hep-ex].

[3] ATLAS Collaboration, *Measurements of Higgs boson production and couplings in diboson final states with the ATLAS detector at the LHC*, Phys. Lett. **B726** (2013) 88–119, arXiv:1307.1427 [hep-ex].

[4] ATLAS Collaboration, *Evidence for the spin-0 nature of the Higgs boson using ATLAS data*, Phys. Lett. **B726** (2013) 120–144, arXiv:1307.1432 [hep-ex].

[5] CMS Collaboration, *Evidence for the direct decay of the 125 GeV Higgs boson to fermions*, Nature Phys. **10** (2014), arXiv:1401.6527 [hep-ex].

[6] CMS Collaboration, *Measurement of the properties of a Higgs boson in the four-lepton final state*, Phys.Rev. **D89** (2014) 092007, arXiv:1312.5353 [hep-ex].

[7] CMS Collaboration, *Measurement of Higgs boson production and properties in the WW decay channel with leptonic final states*, JHEP **1401** (2014) 096, arXiv:1312.1129 [hep-ex].

[8] F. Englert and R. Brout, *Broken symmetry and the mass of gauge vector mesons*, Phys. Rev. Lett. **13** (1964) 321–323.

[9] P. W. Higgs, *Broken symmetries, massless particles and gauge fields*, Phys. Lett. **12** (1964) 132–133.

[10] P. W. Higgs, *Broken symmetries and the masses of gauge bosons*, Phys. Rev. Lett. **13** (1964) 508–509.

[11] P. W. Higgs, *Spontaneous symmetry breakdown without massless bosons*, Phys. Rev. **145** (1966) 1156–1163.

[12] G. Guralnik, C. Hagen, and T. Kibble, *Global conservation laws and massless particles*, Phys. Rev. Lett. **13** (1964) 585–587.

[13] T. Kibble, *Symmetry breaking in non-Abelian gauge theories*, Phys. Rev. **155** (1967) 1554–1561.

[14] A. Djouadi, *The Anatomy of electro-weak symmetry breaking. II. The Higgs bosons in the minimal supersymmetric model*, Phys.Rept. **459** (2008) 1–241, arXiv:hep-ph/0503173 [hep-ph].

[15] G. Branco, P. Ferreira, L. Lavoura, M. Rebelo, M. Sher, et al., *Theory and phenomenology of two-Higgs-doublet models*, Phys. Rept. **516** (2012) 1–102, arXiv:1106.0034 [hep-ph].

[16] P. Fayet, *Supersymmetry and Weak, Electromagnetic and Strong Interactions*, Phys. Lett. **B64** (1976) 159.

[17] P. Fayet, *Spontaneously Broken Supersymmetric Theories of Weak, Electromagnetic and Strong Interactions*, Phys. Lett. **B69** (1977) 489.

[18] G. R. Farrar and P. Fayet, *Phenomenology of the Production, Decay, and Detection of New Hadronic States Associated with Supersymmetry*, Phys. Lett. **B76** (1978) 575–579.

[19] P. Fayet, *Relations Between the Masses of the Superpartners of Leptons and Quarks, the Goldstino Couplings and the Neutral Currents*, Phys. Lett. **B84** (1979) 416.

[20] S. Dimopoulos and H. Georgi, *Softly Broken Supersymmetry and SU(5)*, Nucl. Phys. **B193** (1981) 150.

[21] M. Carena, S. Heinemeyer, O. Stl, C. Wagner, and G. Weiglein, *MSSM Higgs Boson Searches at the LHC: Benchmark Scenarios after the Discovery of a Higgs-like Particle*, Eur. Phys. J. **C73** (2013) 2552, arXiv:1302.7033 [hep-ph].

[22] P. Bechtle, S. Heinemeyer, O. Stal, T. Stefaniak, G. Weiglein, et al., *MSSM Interpretations of the LHC Discovery: Light or Heavy Higgs?*, Eur.Phys.J. **C73** (2013) 2354, arXiv:1211.1955 [hep-ph].

[23] A. Arbey, M. Battaglia, A. Djouadi, and F. Mahmoudi, *The Higgs sector of the phenomenological MSSM in the light of the Higgs boson discovery*, JHEP **1209** (2012) 107, arXiv:1207.1348 [hep-ph].

[24] ALEPH, DELPHI, L3, and OPAL Collaborations, *Search for neutral MSSM Higgs bosons at LEP*, Eur. Phys. J. **C47** (2006) 547–587, arXiv:hep-ex/0602042 [hep-ex].

[25] TNPWG (Tevatron New Physics Higgs Working Group), CDF and D0 Collaborations, *Combined CDF and D0 upper limits on MSSM Higgs boson production in $\tau\tau$ final states with up to 2.2 fb^{-1}*, arXiv:1003.3363 [hep-ex].

[26] CDF Collaboration, T. Aaltonen et al., *Search for Higgs bosons predicted in two-Higgs-doublet models via decays to τ lepton pairs in 1.96 TeV proton–antiproton collisions*, Phys. Rev. Lett. **103** (2009) 201801, arXiv:0906.1014 [hep-ex].

[27] D0 Collaboration, V. M. Abazov et al., *Search for Higgs bosons decaying to τ pairs in $p\bar{p}$ collisions with the D0 detector*, Phys. Rev. Lett. **101** (2008) 071804, arXiv:0805.2491 [hep-ex].

[28] ATLAS Collaboration, *Search for the neutral Higgs bosons of the Minimal Supersymmetric Standard Model in pp collisions at $\sqrt{s} = 7$ TeV with the ATLAS detector*, JHEP **1302** (2013) 095, arXiv:1211.6956 [hep-ex].

[29] CMS Collaboration, *Search for neutral Higgs bosons decaying to τ pairs in pp collisions at $\sqrt{s}$=7 TeV*, Phys. Lett. **B 713** (2012) 68, arXiv:1202.4083 [hep-ex].

[30] R. Aaij et al. (LHCb Collaboration), *Limits on neutral Higgs boson production in the forward region in pp collisions at $\sqrt{s} = 7$ TeV*, JHEP **1305** (2013) 132, arXiv:1304.2591 [hep-ex].

[31] ATLAS Collaboration, *The ATLAS experiment at the CERN Large Hadron Collider*, JINST **3** (2008) S08003.

[32] S. Heinemeyer, W. Hollik, and G. Weiglein, *Constraints on tan Beta in the MSSM from the upper bound on the mass of the lightest Higgs boson*, JHEP **0006** (2000) 009, arXiv:hep-ph/9909540 [hep-ph].

[33] M. Carena, S. Heinemeyer, C. E. M. Wagner and G. Weiglein, *Suggestions for benchmark scenarios for MSSM Higgs boson searches at hadron colliders*, Eur. Phys. J. **C 26** (2003) 601, arXiv:hep-ph/0202167 [hep-ph].

[34] ATLAS collaboration, *Evidence for Higgs Boson Decays to the $\tau\tau$ Final State with the ATLAS Detector*, ATLAS-CONF-2013-108, available at http://cds.cern.ch/record/1632191.

[35] CMS Collaboration, *Evidence for the 125 GeV Higgs boson decaying to a pair of τ leptons*, JHEP **1405** (2014) 104, arXiv:1401.5041 [hep-ex].

[36] ATLAS Collaboration, *The ATLAS simulation infrastructure*, Eur. Phys. J. **C70** (2010) 823–874, arXiv:1005.4568 [physics.ins-det].

[37] GEANT4 Collaboration, S. Agostinelli et al., *GEANT4 - a simulation toolkit*, Nucl. Instrum. Meth. **A506** (2003) 250–303.

[38] M. Spira, *HIGLU: A program for the calculation of the total Higgs production cross section at hadron colliders via gluon fusion including QCD corrections*, arXiv:hep-ph/9510347 [hep-ph].

[39] R. V. Harlander and W. B. Kilgore, *Next-to-Next-to-Leading Order Higgs Production at Hadron Colliders*, Phys. Rev. Lett. **88** (2002) 201801, arXiv:hep-ph/0201206 [hep-ph].

[40] R. V. Harlander, S. Liebler, and H. Mantler, *SusHi: A program for the calculation of Higgs production in gluon fusion and bottom-quark annihilation in the Standard Model and the MSSM*, Computer Physics Communications **184** (2013) 1605–1617, arXiv:1212.3249 [hep-ph].

[41] S. Dittmaier, M. Krämer and M. Spira, *Higgs radiation off bottom quarks at the Tevatron and the LHC*, Phys. Rev. **D70** (2004) 074010, arXiv:hep-ph/0309204 [hep-ph].

[42] S. Dawson, C. B. Jackson, L. Reina and D. Wackeroth, *Exclusive Higgs boson production with bottom quarks at hadron colliders*, Phys. Rev. **D69** (2004) 074027, arXiv:hep-ph/0311067 [hep-ph].

[43] R. Harlander and W. B. Kilgore, *Higgs boson production in bottom quark fusion at next-to-next-to-leading order*, Phys. Rev. **D68** (2003) 013001, arXiv:hep-ph/0304035 [hep-ph].

[44] R. Harlander, M. Kramer, and M. Schumacher, *Bottom-quark associated Higgs-boson production: reconciling the four- and five-flavour scheme approach*, arXiv:1112.3478 [hep-ph].

[45] M. Frank, T. Hahn, S. Heinemeyer, W. Hollik, H. Rzehak and G. Weiglein, *The Higgs boson masses and mixings of the complex MSSM in the Feynman-diagrammatic approach*, JHEP **0702** (2007) 047, arXiv:hep-ph/0611326 [hep-ph].

[46] S. Alioli, P. Nason, C. Oleari, and E. Re, *NLO Higgs boson production via gluon fusion matched with shower in POWHEG*, JHEP **0904** (2009) 002, arXiv:0812.0578 [hep-ph].

[47] T. Gleisberg, S. Hoeche, F. Krauss, M. Schoenherr, S. Schumann, F. Siegert and J. Winter, *Event generation with SHERPA 1.1*, JHEP **0902** (2009) 007, arXiv:0811.4622 [hep-ph].

[48] H.-L. Lai, M. Guzzi, J. Huston, Z. Li, P. M. Nadolsky, et al., *New parton distributions for collider physics*, Phys. Rev. **D82** (2010) 074024, arXiv:1007.2241 [hep-ph].

[49] M. L. Mangano, M. Moretti, F. Piccinini, R. Pittau and A. D. Polosa, *ALPGEN, a generator for hard multiparton processes in hadronic collisions*, JHEP **0307** (2003) 001, arXiv:hep-ph/0206293 [hep-ph].

[50] T. Sjöstrand, S. Mrenna and P. Skands, *PYTHIA 6.4 physics and manual*, JHEP **0605** (2006) 026, arXiv:hep-ph/0603175 [hep-ph].

[51] T. Sjostrand, S. Mrenna, and P. Z. Skands, *A Brief Introduction to PYTHIA 8.1*, Comput. Phys. Commun. **178** (2008) 852–867, arXiv:0710.3820 [hep-ph].

[52] G. Corcella et al., *HERWIG 6.5: an event generator for hadron emission reactions with interfering gluons (including supersymmetric processes)*, JHEP **0101** (2001) 010, arXiv:hep-ph/0011363 [hep-ph].

[53] S. Frixione and B. R. Webber, *Matching NLO QCD computations and parton shower simulations*, JHEP **0206** (2002) 029, arXiv:hep-ph/0204244 [hep-ph].

[54] B. P. Kersevan and E. Richter-Wąs, *The Monte Carlo event generator AcerMC version 2.0 with interfaces to PYTHIA 6.2 and HERWIG 6.5*, arXiv:hep-ph/0405247 [hep-ph].

[55] J. Pumplin, D. Stump, J. Huston, H. Lai, P. M. Nadolsky, et al., *New generation of parton distributions with uncertainties from global QCD analysis*, JHEP **0207** (2002) 012, arXiv:hep-ph/0201195 [hep-ph].

[56] S. Jadach, J. H. Kuhn and Z. Was, *TAUOLA - a library of Monte Carlo programs to simulate decays of polarized τ leptons*, Comput. Phys. Commun. **64** (1990) 275–299.

[57] E. Barberio, B. V. Eijk and Z. Was, *PHOTOS - a universal Monte Carlo for QED radiative corrections in decays*, Comput. Phys. Commun. **66** (1991) 115–128.

[58] ATLAS Collaboration, *Search for the Standard Model Higgs boson in the $H \to \tau\tau$ decay mode in $\sqrt{s}$=7 TeV pp collisions with ATLAS*, JHEP **1209** (2012) 070, arXiv:1206.5971 [hep-ex].

[59] ATLAS Collaboration, *Electron efficiency measurements with the ATLAS detector using the 2012 LHC proton-proton collision data*, ATLAS-CONF-2014-032, available at http://cdsweb.cern.ch/record/1706245.

[60] ATLAS Collaboration, *Measurement of the muon reconstruction performance of the ATLAS detector using 2011 and 2012 LHC proton-proton collision data*, arXiv:1407.3935 [hep-ex].

[61] M. Cacciari, G. P. Salam and G. Soyez, *The anti-k_t jet clustering algorithm*, JHEP **0804** (2008) 063, arXiv:0802.1189 [hep-ph].

[62] W. Lampl et al., *Calorimeter Clustering Algorithms: Description and Performance*, ATL-LARG-PUB-2008-002, CERN, Geneva Switzerland (2008).

[63] ATLAS Collaboration, *Jet energy measurement and its systematic uncertainty in proton-proton collisions at $\sqrt{s}$ = 7 TeV with the ATLAS detector*, arXiv:1406.0076 [hep-ex].

[64] ATLAS collaboration, *Calibration of b-tagging using dileptonic top pair events in a combinatorial likelihood approach with the ATLAS experiment*, ATLAS-CONF-2014-004, available at http://cds.cern.ch/record/1664335.

[65] ATLAS collaboration, *Calibration of the performance of b-tagging for c and light-flavour jets in the 2012 ATLAS data*, ATLAS-CONF-2014-046, available at http://cds.cern.ch/record/1741020.

[66] ATLAS collaboration, *Identification of the Hadronic Decays of Tau Leptons in 2012 Data with the ATLAS Detector*, ATLAS-CONF-2013-064, available at http://cds.cern.ch/record/1562839.

[67] ATLAS Collaboration, *Performance of missing transverse momentum reconstruction in proton–proton collisions at 7 TeV with ATLAS*, Eur. Phys. J. **C72** (2012) 1844, arXiv:1108.5602 [hep-ex].

[68] A. Elagin, P. Murat, A. Pranko and A. Safonov, *A new mass reconstruction technique for resonances decaying to di-τ*, Nucl. Instrum. Meth. **A654** (2011) 481–489, arXiv:1012.4686 [hep-ex].

[69] C. Anastasiou, L. J. Dixon, K. Melnikov, and F. Petriello, *High precision QCD at hadron colliders: Electroweak gauge boson rapidity distributions at NNLO*, Phys. Rev. **D69** (2004) 094008, arXiv:hep-ph/0312266 [hep-ph].

[70] LHC Higgs Cross Section Working Group, *Handbook of LHC Higgs Cross Sections: 1. Inclusive Observables*, arXiv:1101.0593 [hep-ph].

[71] ATLAS Collaboration, *Improved luminosity determination in pp collisions at $\sqrt{s}$ = 7 TeV using the ATLAS detector at the LHC*, Eur. Phys. J. **C73** (2013) 2518, arXiv:1302.4393 [hep-ex].

[72] ATLAS collaboration, *Performance of the ATLAS tau trigger in 2011*, ATLAS-CONF-2013-006, available at http://cds.cern.ch/record/1510157.

[73] ATLAS collaboration, *Determination of the tau energy scale and the associated systematic uncertainty in proton-proton collisions at $\sqrt{s}$ = 8 TeV with the ATLAS detector at the LHC in 2012*, ATLAS-CONF-2013-044, available at http://cds.cern.ch/record/1544036.

[74] ATLAS Collaboration, *Jet energy resolution in proton-proton collisions at $\sqrt{s}$ = 7 TeV recorded in 2010 with the ATLAS detector*, Eur. Phys. J. **C73** (2013) 2306, arXiv:1210.6210 [hep-ex].

[75] ATLAS Collaboration, *Performance of Missing Transverse Momentum Reconstruction in ATLAS studied in Proton-Proton Collisions recorded in 2012 at 8 TeV*, ATLAS-CONF-2013-082, available at http://cdsweb.cern.ch/record/1570993.

[76] ATLAS Collaboration, *Electron reconstruction and identification efficiency measurements with the ATLAS detector using the 2011 LHC proton-proton collision data*, arXiv:1404.2240 [hep-ex].

[77] ATLAS Collaboration, *Electron and photon energy calibration with the ATLAS detector using LHC Run 1 data*, arXiv:1407.5063 [hep-ex].

[78] A. L. Read, *Presentation of search results: the CL_s technique*, J. Phys. **G28** (2002) 2693–2704.

[79] G. Cowan, K. Cranmer, E. Gross and O. Vitells, *Asymptotic formulae for likelihood-based tests of new physics*, Eur. Phys. J. **C71** (2011) 1554, arXiv:1007.1727 [physics.data-an].

A Additional Figures and Tables

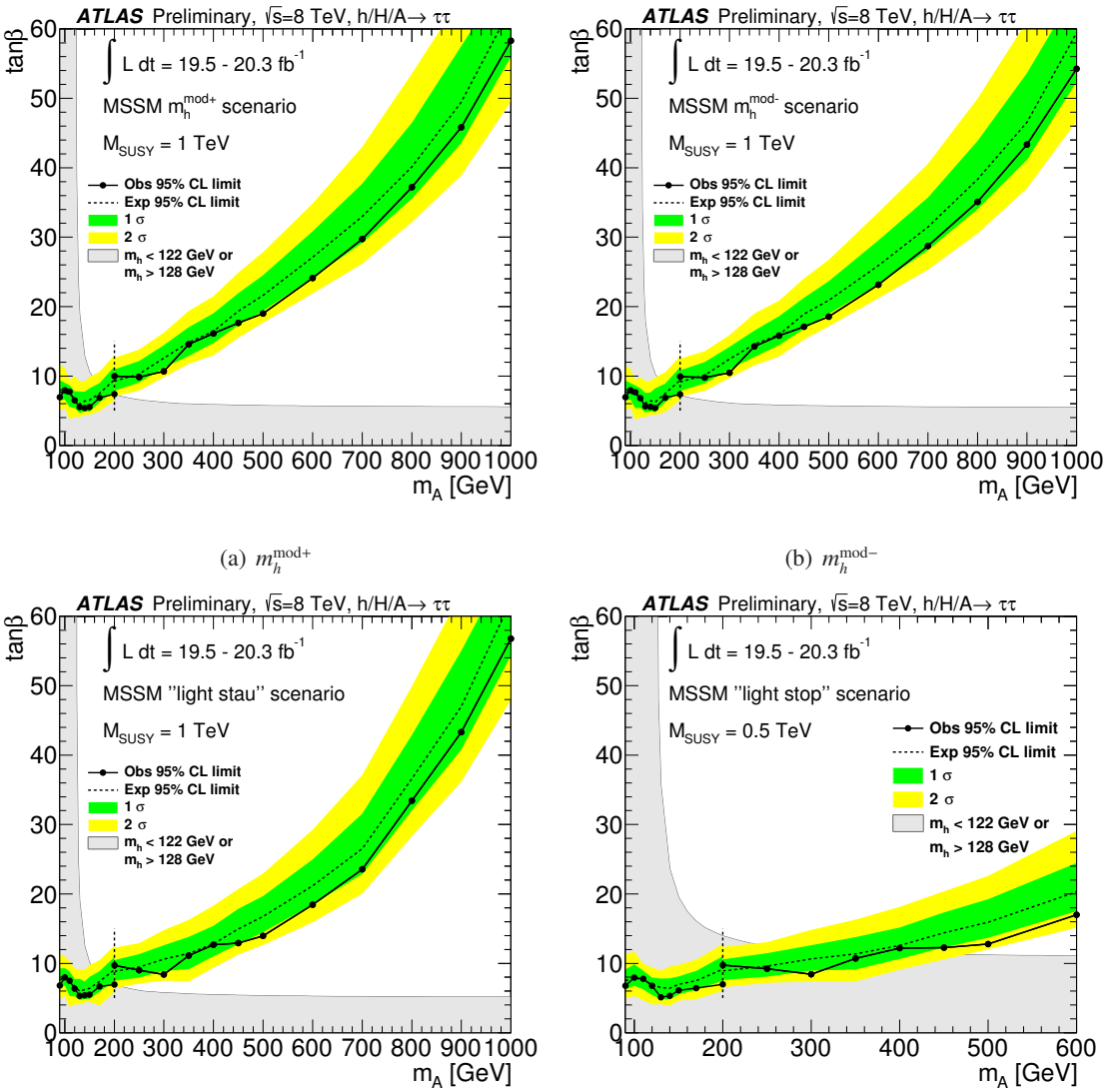

(a) $m_h^{\text{mod+}}$

(b) $m_h^{\text{mod-}}$

(c) light stau

(d) light stop

Figure 8: Expected (dashed line) and observed (solid line with markers) 95% CL upper limits on $\tan\beta$ as a function of m_{A}. Values of $\tan\beta$ greater than the shown lines are excluded. The upper limits are shown in for the statistical combination of all channels in various MSSM benchmark scenarios. The vertical dashed line at 200 GeV indicates the transition point between low and high mass categories. These scenarios are defined as described in Ref. [21], apart from the "light stop" scenario that has been modified such that the gaugino mass parameters are $M_1 = 340$ GeV, $M_2 = 400$ GeV and the Higgsino mass parameter is $\mu = 400$ GeV. In the same figure, the $m_{\text{A}} - \tan\beta$ plane region which is incompatible with a light, CP-even Higgs boson with mass in the range 122–128 GeV is shown.

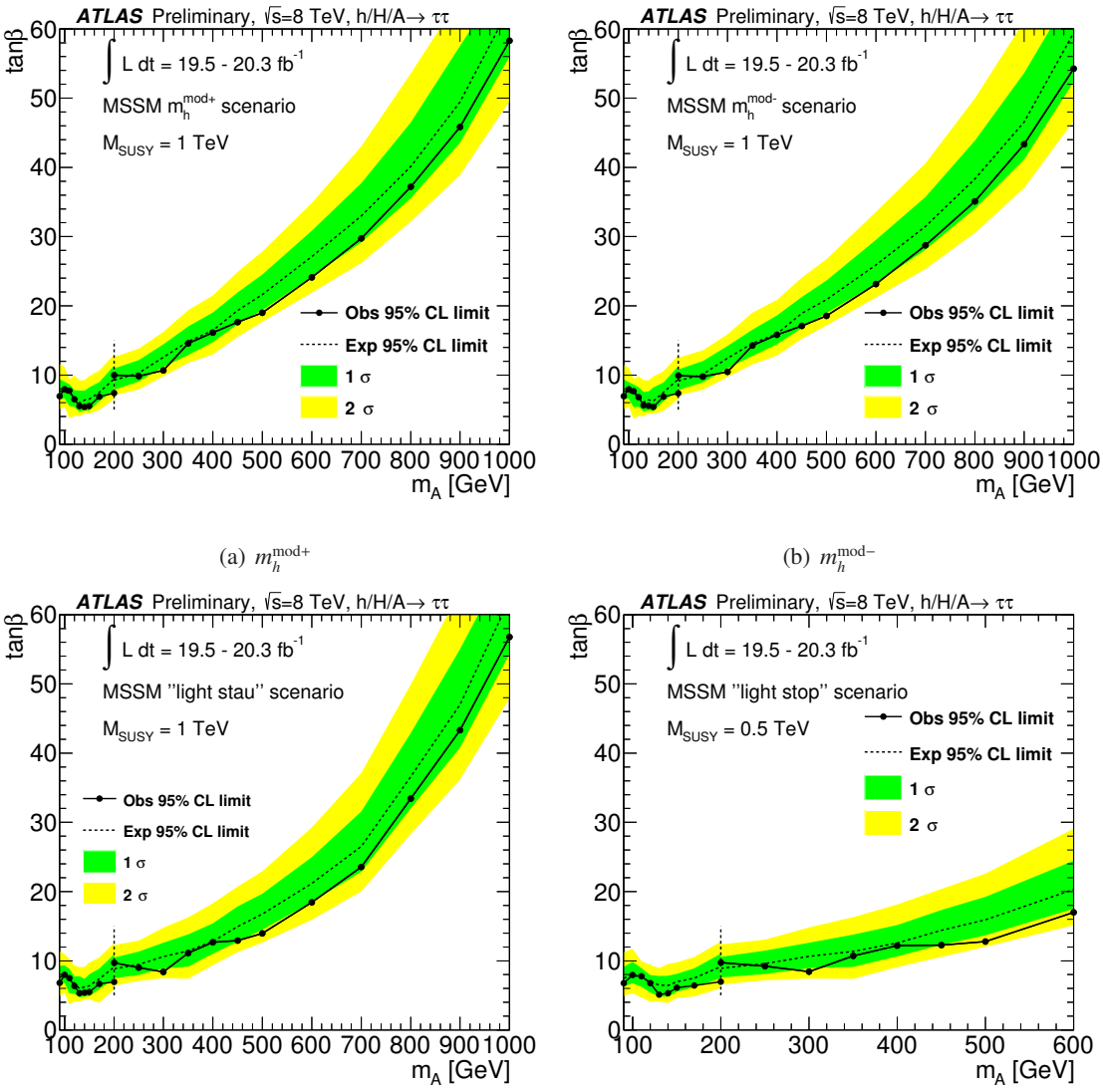

(a) $m_h^{\mathrm{mod+}}$

(b) $m_h^{\mathrm{mod-}}$

(c) light stau

(d) light stop

Figure 9: Expected (dashed line) and observed (solid line with markers) 95% CL upper limits on $\tan\beta$ as a function of m_{A}. Values of $\tan\beta$ greater than the shown lines are excluded. The upper limits are shown in for the statistical combination of all channels in four alternative MSSM benchmark scenarios. The vertical dashed line at 200 GeV indicates the transition point between low and high mass categories. These scenarios are defined as described in Ref. [21] to account for the observation of a H boson at $\sim$ 125 GeV, apart from the "light stop" scenario that has been modified such that the gaugino mass parameters are $M_1 = 340$ GeV, $M_2 = 400$ GeV and the Higgsino mass parameter is $\mu = 400$ GeV.

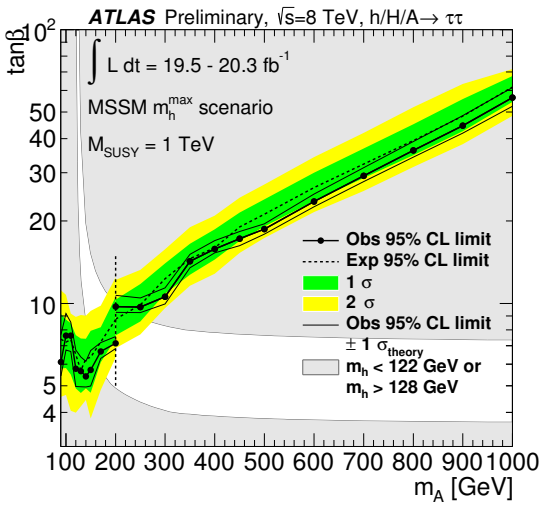

Figure 10: Expected (dashed line) and observed (solid line with markers) 95% CL upper limits on $\tan\beta$ as a function of m_{A} for the MSSM m_h^{max} scenario with the $\tan\beta$ axis in logarithmic scale. The vertical dashed line at 200 GeV indicates the transition point between low and high mass categories in the $\tau_{\mathrm{lep}}\tau_{\mathrm{had}}$ channel. In the same figure, the $m_{\mathrm{A}}-\tan\beta$ plane region which is incompatible with a light, CP-even Higgs boson with mass in the range 122–128 GeV is shown.

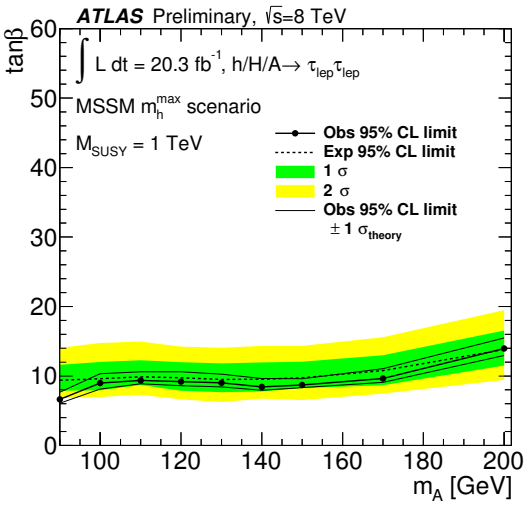

(a) $m_h^{\max}$, $\tau_{\text{lep}}\tau_{\text{lep}}$

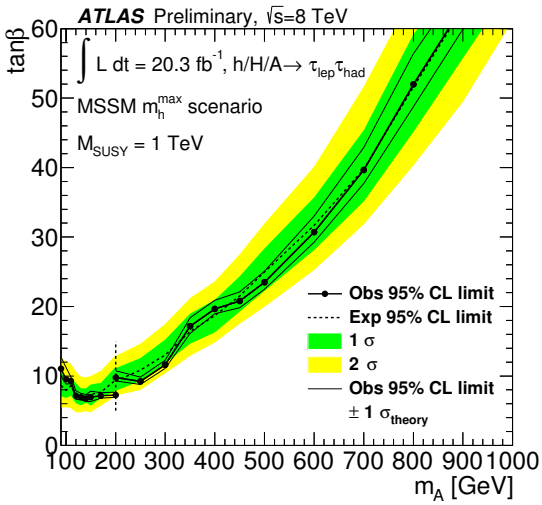

(b) $m_h^{\max}$, $\tau_{\text{lep}}\tau_{\text{had}}$

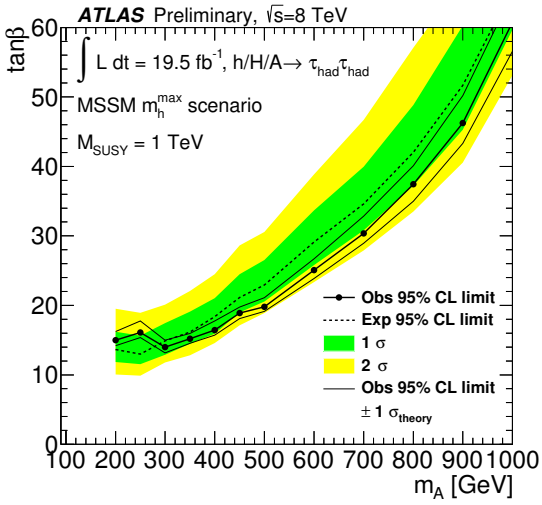

(c) $m_h^{\max}$, $\tau_{\text{had}}\tau_{\text{had}}$

Figure 11: Expected (dashed line) and observed (solid line with markers) 95% CL upper limits on $\tan\beta$ as a function of m_{A} for the MSSM $m_h^{\max}$ scenario. Values of $\tan\beta$ greater than the shown lines are excluded. The upper limits are shown separately for $\tau_{\text{lep}}\tau_{\text{lep}}$ channel in (a), $\tau_{\text{lep}}\tau_{\text{had}}$ channel in (b) and $\tau_{\text{had}}\tau_{\text{had}}$ channel in (c). The vertical dashed line at 200 GeV in (b) indicates the transition point between low and high mass categories in the $\tau_{\text{lep}}\tau_{\text{had}}$ channel.

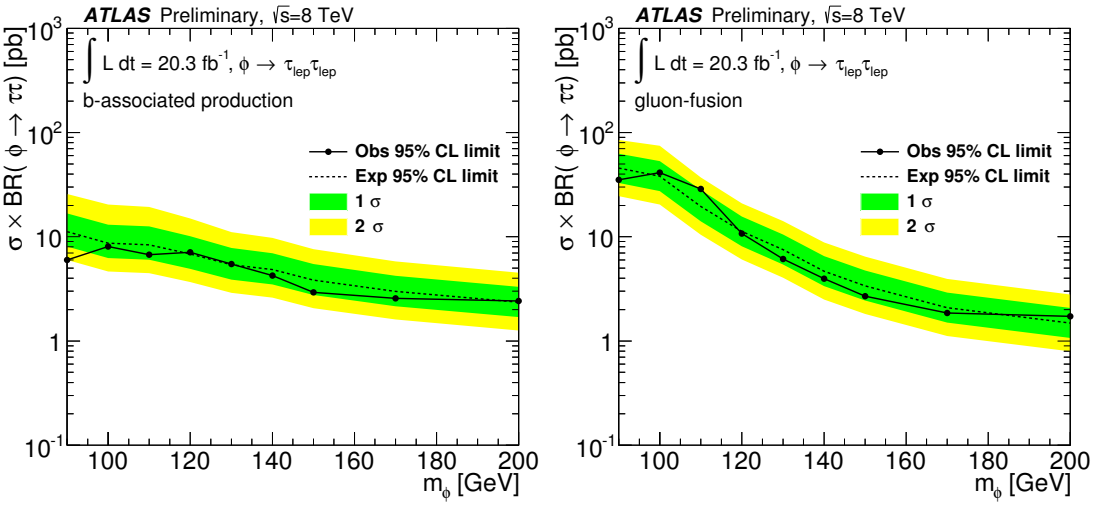

(a) $\tau_{\text{lep}}\tau_{\text{lep}}$

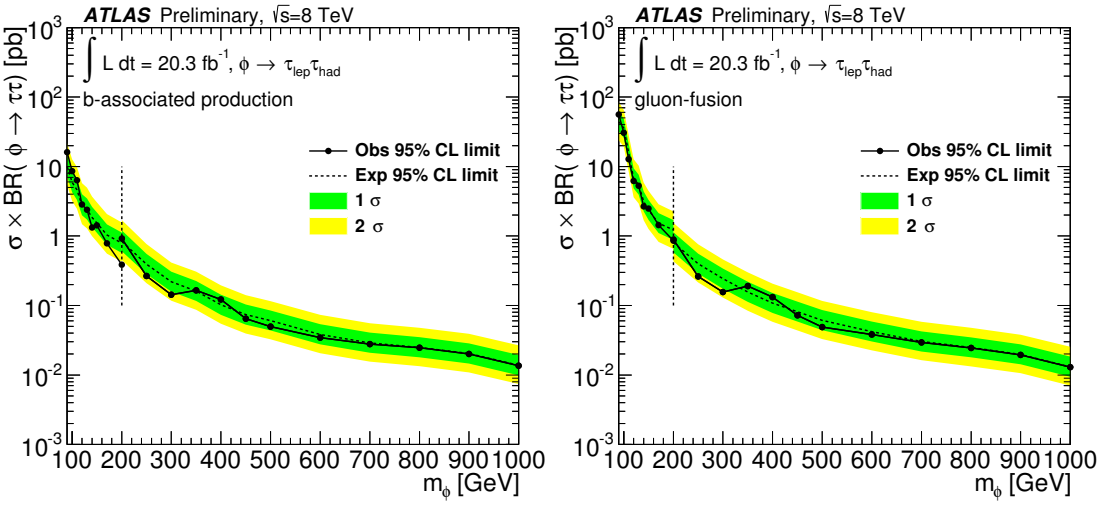

(b) $\tau_{\text{lep}}\tau_{\text{had}}$

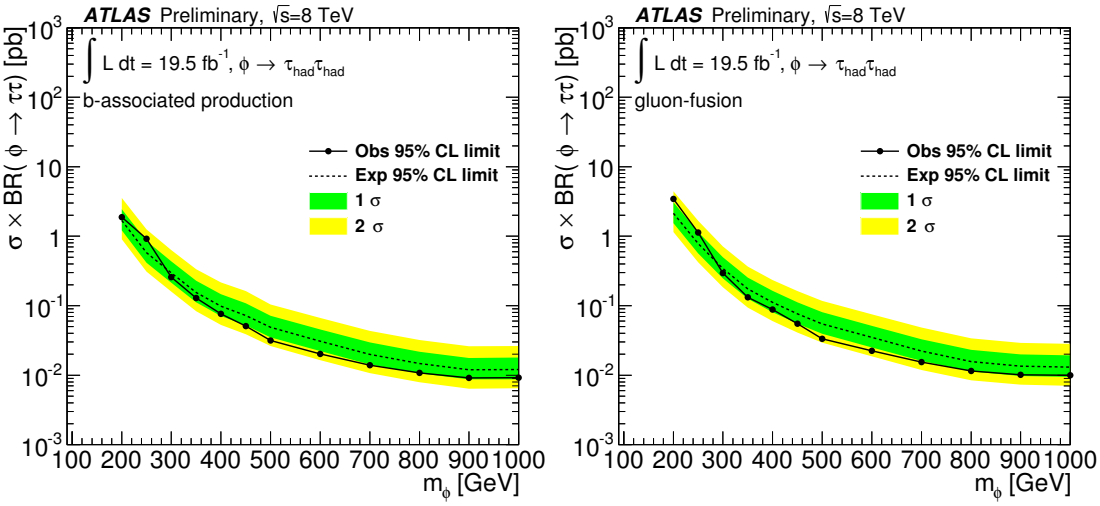

(c) $\tau_{\text{had}}\tau_{\text{had}}$

Figure 12: Expected (dashed line) and observed (solid line with markers) 95% CL upper limits on the cross section for gluon-fusion and *b*-associated Higgs boson production times the branching ratio into τ pairs for each channel separately.